Int. J. Multiphase Flow Vol. 14, No. 1, pp. 67–79, 1988
Printed in Great Britain.

0301-9322/88 $3.00 + 0.00

LINEAR CAPILLARY INSTABILITY OF COMPOUND JETS

S. RADEV and B. TCHAVDAROV
Institute of Mechanics and Biomechanics, Bulgarian Academy of Sciences, 1090 Sofia, P.O. Box 373, Bulgaria

(*Received* 29 *September* 1986; *in revised form* 7 *July* 1987)

Abstract—The capillary instability of compound jets has been studied using a linear model derived from the two-dimensional equations of motion. The flow was considered as a superposition of steady-state plug flow and travelling waves of small amplitude. The eigenvalue problem, obtained via the disturbance-phase velocity, was solved numerically and the analysis applied to compound jets of liquids with different surface tensions, densities and viscosities. The influence of the outer secondary-fluid layer on the compound jet instability was analysed. Three different break-up regimes were established and the distance to the first break-up point was predicted. The necessary qualitative conditions for manifesting a specific break-up regime were identified, and the numerical results compared, whenever possible, with the experimental data available.

1. INTRODUCTION

The new ink-jet printing method, the compound jet, was developed at the Lund Institute of Technology, Sweden (Hermanrud & Hertz 1979; Hermanrud 1981). The compound jet is generated by a single jet emerging from a nozzle below the surface of another stationary fluid. After breaking the surface the jet consists of a cylindrical core (primary jet) surrounded by a co-axial layer of the secondary fluid. The compound jet generation principles and a qualitative description of the hydrodynamics of the jet have been given by Hertz & Hermanrud (1983). Radev & Gospodinov (1986) studied numerically the steady compound jet flow in a boundary-layer approximation: as they pointed out, shortly after emerging into the air, the compound jet attains uniform velocity and constant radii.

Three different types of compound jet instability were observed by Hertz & Hermanrud (1983): capillary, sinuous and varicose instability. The first theoretical investigations of compound jet instability were performed using a linear analysis of the one-dimensional equations of motion for both phases—assumed inviscid [capillary instability, Sanz & Meseguer (1985) and Radev & Shkadov (1985); sinuous instability, Radev (1986)]. Shutov (1985), studying capillary instability, obtained asymptotic solutions for inviscid and heavy-viscous compound liquid columns in the case of thin secondary-fluid layer.

The purpose of this paper is to study capillary instability including viscosity in the problem by means of a model derived from the two-dimensional equations of motion. The analysis of compound jet instability in this more general case requires extensive use of numerical methods. An efficient initial-value technique is applied to solve the problem. The influence of the secondary-fluid layer on the instability is analysed numerically. Depending on the physical properties of both compound jet phases, the jet radii and velocity, three different break-up regimes are possible. The necessary qualitative conditions for existence of the various break-up regimes are established by means of a variety of numerical experiments.

2. GENERAL EQUATION OF THE MODEL

The instability of a compound liquid jet of constant radii R_j and uniform velocity U is considered (see figure 1). Hereafter the subscript $j = 1$ is set for the primary jet (inner fluid), whereas $j = 2$ denotes the secondary-fluid layer (outer fluid); anywhere where the subscript j is used in the text, $j = 1, 2$. Both phases are assumed to be viscous, incompressible Newtonian liquids. The interaction with ambient air is neglected. The flow is considered to be two-dimensional and axisymmetric. A

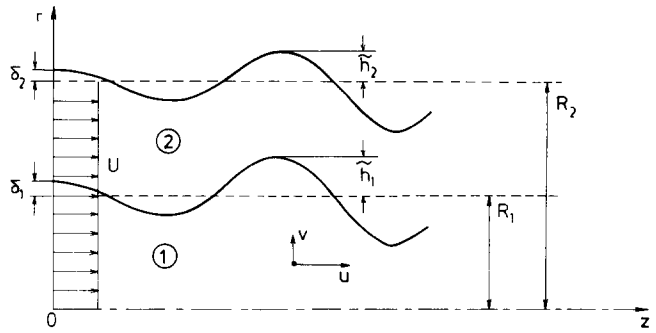

Figure. 1. Flow configuration of the compound jet and coordinate system. The flow is considered as a superposition of plug flow and travelling waves of small amplitude in the streamwise direction. ① primary jet; ② secondary-fluid layer.

cylindrical coordinate system (r, z) is initiated such that the z-axis coincides with the axis of the jet.

We impose upon this initially steady motion arbitrary, small, two-dimensional disturbances $\tilde{u}_j(r, z, t)$, $\tilde{v}_j(r, z, t)$, $\tilde{p}_j(r, z, t)$, $\tilde{h}_j(z, t)$, i.e.

$$u_j = U + \tilde{u}_j, \quad v_j = \tilde{v}_j, \quad h_j = R_j + \tilde{h}_j, \quad p_j = P_j + \tilde{p}_j,$$

where t is time variable, u_j and v_j are the velocities in the z- and r-directions, respectively, h_j are the jet radii, p_j are the pressures and P_j are the corresponding undisturbed values.

Neglecting all terms of second order in the disturbance quantities, we obtain the linearized equations of motion and continuity:

$$\frac{\partial \tilde{\mathbf{u}}_j}{\partial t} + U\frac{\partial \tilde{\mathbf{u}}_j}{\partial z} = -\frac{1}{\rho_j}\nabla \tilde{p}_j + \frac{\mu_j}{\rho_j}\nabla^2 \tilde{\mathbf{u}}_j; \qquad [1]$$

and

$$\nabla \cdot \tilde{\mathbf{u}}_j = 0, \quad \tilde{\mathbf{u}}_j = (\tilde{u}_j, \tilde{v}_j); \qquad [2]$$

where μ_j and ρ_j are viscosity and density, respectively.

At the jet axis of symmetry we have

$$\tilde{v}_1 = 0, \quad \frac{\partial \tilde{u}_1}{\partial r} = 0, \quad r = 0. \qquad [3]$$

The boundary conditions to be applied at the surface h_j, which can be taken as $r \sim R_j$ to first order in $\tilde{h}_j$, require that there be no net flux of mass across the surfaces and that the velocity as well as the shear and normal stresses be continuous. These boundary conditions give, respectively:

$$\left.\begin{aligned} \tilde{v}_j &= \frac{\partial \tilde{h}_j}{\partial t} + U\frac{\partial \tilde{h}_j}{\partial z}, && r = R_j, \\ \tilde{u}_1 &= \tilde{u}_2, \quad \tilde{v}_1 = \tilde{v}_2, && r = R_1, \\ \left[\frac{\partial \tilde{u}}{\partial r} + \frac{\partial \tilde{v}}{\partial z}\right]_j^{j+1} &= 0, && r = R_j, \\ \left[\tilde{p} - 2\mu\frac{\partial \tilde{v}}{\partial z}\right]_j^{j+1} &= \frac{\sigma_j}{R_j^2}\left(\tilde{h}_j + R_j^2\frac{\partial^2 \tilde{h}_j}{\partial z^2}\right), && r = R_j, \end{aligned}\right\} \qquad [4]$$

where $[\cdot]_j^{j+1}$ denotes the jump of the quantity in brackets, crossing the interface $r = R_j$ in the r-direction, i.e. $[\cdot]_j^{j+1} = (\cdot)_{j+1} - (\cdot)_j$ at $r = R_j$. When the interaction with the ambient medium is

neglected $(\cdot)_3$ is always zero. The last boundary conditions of [4] express the effect of the surface tensions σ_j.

A stream function $\tilde{\psi}_j$ is defined such that

$$\tilde{u}_j = \frac{1}{r}\frac{\partial}{\partial r}(r\tilde{\psi}_j), \quad \tilde{v}_j = -\frac{\partial \tilde{\psi}_j}{\partial z}. \tag{5}$$

If we assume the disturbances to be symmetric about the jet axis, then $\tilde{\psi}_j$, $\tilde{h}_j$ and $\tilde{p}_j$ may be written as Fourier series involving terms of the form

$$\tilde{\psi}_j = \bar{\psi}_j(r)\exp\xi, \quad \tilde{h}_j = \bar{h}_j \exp\xi, \quad \tilde{p}_j = \bar{p}_j(r)\exp\xi, \quad \xi = i\bar{\alpha}(z - \bar{c}t), \tag{6}$$

where $\bar{\psi}_j$, $\bar{h}_j$ and $\bar{p}_j$ are the corresponding Fourier amplitudes. This representation [6] of the disturbances is the so-called travelling wave of phase velocity $\bar{c}$ and wavenumber $\bar{\alpha}$.

Introducing non-dimensional variables by using R_1 and U as a characteristic scale, one easily finds that in terms of the dimensionless variable $\phi_j = \bar{\psi}_j/R_1 U$, [1] and boundary conditions [3] and [4] give, respectively:

$$i\alpha\,\mathrm{Re}_1(1-c)(L-\alpha^2)\phi_j = \frac{\mu_j\rho_1}{\rho_j\mu_1}(L-\alpha^2)^2\phi_j; \tag{7}$$

$$L\phi_j \equiv \frac{\mathrm{d}^2\phi_j}{\mathrm{d}r^2} + \frac{1}{r}\frac{\mathrm{d}\phi_j}{\mathrm{d}r} - \frac{1}{r^2}\phi_j \equiv \left(\frac{1}{r}(r\phi_j)'\right)'; \tag{8}$$

$$\left.\begin{aligned}
\phi_1 = \phi_1'' = 0, \quad & r = 0,\\
[\mu(L+\alpha^2)\phi]_j^{j+1} = 0, \quad & r = r_j,\\
\phi_1 = \phi_2, \quad \phi_1' = \phi_2', \quad & r = r_1,\\
(i\alpha\mu_1\,\mathrm{Re}_1)^{-1}\left[\mu\left\{\frac{1}{r}(rL\phi)' - \frac{\alpha^2}{r}(r\phi)' - 2\alpha^2\phi'\right\}\right]_j^{j+1} - \frac{1-c}{\rho_1}\left[\frac{\rho}{r}(r\phi)'\right]_j^{j+1} = S_jH_j, \quad & r = r_j,\\
H_j = -\frac{\phi_j}{1-c}, \quad S_j = \frac{\sigma_j}{\sigma_1}\frac{1-\alpha^2 r_j^2}{\mathrm{We}_1 r_j^2}; &
\end{aligned}\right\} \tag{9}$$

where $r_j = R_j/R_1$, $H_j = \bar{h}_j/R_1$, $\alpha = \bar{\alpha}R_1$ and $c = \bar{c}/U$ are new dimensionless variables: $\mathrm{Re}_1 = \rho_1 R_1 U/\mu_1$ and $\mathrm{We}_1 = \rho_1 R_1 U^2/\sigma_1$ are the Reynolds and Weber numbers, respectively.

Problem [7]–[9] is an eigenvalue problem for the Orr–Sommerfeld equations [7] about the complex phase velocity c when the wavenumber α is given a real value. When $\mathscr{I}m\, c > 0$, the disturbance of wavelength $\lambda = 2\pi/\alpha$ grows in time with exponential rate $q = \mathscr{I}m(\alpha c)$, i.e. the so-called temporal instability.

If the primary jet and secondary-fluid layer have the same physical properties the boundary conditions at $r = r_1$ can be neglected and [7]–[9] reduce to the classical Weber solution for a single viscous jet.

In the general case, the required eigenvalue relation can also be obtained analytically from the governing equations [7]–[9] in terms of Bessel functions but the relation is too complicated and practically unworkable in the analysis. In the next section a numerical method for solving the eigenvalue problem [7]–[9] is proposed.

3. METHOD OF SOLUTION

If new variables $\mathbf{v}_j = (v_j^{(1)}, v_j^{(2)}, v_j^{(3)}, v_j^{(4)})^{\mathrm{T}}$ are introduced such that

$$v_j^{(1)} = \phi_j, \quad v_j^{(2)} = (L-\alpha^2)\phi_j, \quad v_j^{(3)} = \frac{1}{r}(rv_j^{(1)})', \quad v_j^{(4)} = \frac{1}{r}(rv_j^{(2)})',$$

then problem [7]–[9] is transformed into a system of first-order linear differential equations:

$$\mathbf{v}_j' = \mathbf{M}_j \cdot \mathbf{v}_j, \quad \mathbf{M}_j = \begin{vmatrix} -\frac{1}{r} & 0 & 1 & 0 \\ 0 & -\frac{1}{r} & 0 & 1 \\ \alpha^2 & 1 & 0 & 1 \\ 0 & m_j & 0 & 0 \end{vmatrix}, \quad m_j = \alpha^2 + i\alpha \,\mathrm{Re}_1 \frac{\rho_j \mu_1}{\mu_j \rho_1}(1-c) \tag{10}$$

with homogeneous boundary conditions

$$\left.\begin{aligned} v_1^{(1)} = v_1^{(2)} = 0, \quad & r = 0 \\ v_1^{(1)} = v_2^{(1)}, \quad v_1^{(3)} = v_2^{(3)}, \quad & r = r_1 \\ [\mu(v^{(2)} + 2\alpha^2 v^{(1)})]_j^{j+1} = 0, \quad & r = r_j \\ (i\alpha\mu_1 \,\mathrm{Re}_1)^{-1}\left[\mu\left\{v^{(4)} - 2\alpha^2\left(v^{(3)} - \frac{1}{r}v^{(1)}\right)\right\}\right]_j^{j+1} - \frac{1-c}{\rho_1}[\rho v^{(3)}]_j^{j+1} = \frac{S_j}{1-c}v_j^{(1)}, \quad & r = r_j. \end{aligned}\right\} \tag{11}$$

To solve the eigenvalue problem [10, 11] we use an initial-value technique for boundary-value problems. The conception of the method is given by Tayfer (1973) and Abramov *et al.* (1977).

Let us assume that $\mathbf{v}_j$ $(j = 1, 2)$ is the subset of solutions of [10] which only satisfies the boundary conditions at $r = 0$ and $r = r_2$, respectively. The equations of this subset can be written as

$$\left.\begin{aligned} v_1^{(1)} &= a_1(r)v_1^{(3)} + a_2(r)v_1^{(4)} \\ v_1^{(2)} &= a_3(r)v_1^{(3)} + a_4(r)v_1^{(4)} \end{aligned}\right\} \quad r \in [0, r_1] \tag{12}$$

and

$$\left.\begin{aligned} v_2^{(1)} &= b_1(r)v_2^{(2)} + b_2(r)v_2^{(4)} \\ v_2^{(3)} &= b_3(r)v_2^{(2)} + b_4(r)v_2^{(4)} \end{aligned}\right\} \quad r \in [r_1, r_2], \tag{13}$$

where $a_k(r)$ and $b_k(r)$ $(k = 1, 2, 3, 4)$ are new unknown functions satisfying certain (see [15] and [17] below) initial conditions at $r = 0$ and $r = r_2$ correspondingly, so that $\mathbf{v}_j$ $(j = 1, 2)$ satisfy the boundary conditions at $r = 0$ and $r = r_2$, respectively.

After differentiation of both sides of [12] and [13], using [10], we find that the unknown functions a_k and b_k are governed by initial-value problems as follows:

$$\left.\begin{aligned} a_1' &= 1 - \frac{a_1}{r} - \alpha^2 a_1^2 - a_3(a_1 + m_1 a_2) \\ a_2' &= -\frac{a_2}{r} - \alpha^2 a_1 a_2 - a_4(a_1 + m_1 a_2) \\ a_3' &= -\frac{a_3}{r} - \alpha^2 a_1 a_3 - a_3(a_3 + m_1 a_4) \\ a_4 &= 1 - \frac{a_4}{r} - \alpha^2 a_2 a_3 - a_4(a_3 + m_1 a_4) \end{aligned}\right\} \quad r \in [0, 1], \tag{14}$$

with initial conditions at $r = 0$,

$$a_1 = a_2 = a_3 = a_4 = 0; \tag{15}$$

and

$$\left.\begin{aligned} b_1' &= -m_2 b_2 + b_3 \\ b_2' &= -b_1 - \frac{b_2}{r} + b_4 \\ b_3' &= 1 + \alpha^2 b_1 + \frac{b_3}{r} - m_2 b_4 \\ b_4' &= \alpha^2 b_2 - b_3 \end{aligned}\right\} r \in [r_1, r_2], \qquad [16]$$

with initial conditions at $r = r_2$,

$$\left.\begin{aligned} b_1 &= -\frac{1}{2\alpha^2}, \\ b_2 &= b_1 b_3 \left\{\frac{2\alpha^2}{r} - i\alpha\ \mathrm{Re}_1 \frac{S_2}{\mu_0(1-c)}\right\}, \\ b_3 &= \left\{2\alpha^2 + i\alpha\ \mathrm{Re}_1 \frac{\rho_0}{\mu_0}(1-c)\right\}^{-1}, \\ b_4 &= 0, \end{aligned}\right. \qquad [17]$$

where

$$\mu_0 = \frac{\mu_2}{\mu_1}, \quad \rho_0 = \frac{\rho_2}{\rho_1}.$$

Finally, if $v_j^{(k)}$ are forced to satisfy the boundary conditions at $r = r_1$, we have in terms of $\mathbf{w} = (v_1^{(3)}, v_1^{(4)}, v_2^{(2)}, v_2^{(4)})^{\mathrm{T}}$:

$$\mathbf{K}\cdot\mathbf{w} = 0, \quad r = r_1, \quad \mathbf{K} = \begin{vmatrix} a_1 & a_2 & -b_1 & -b_2 \\ 1 & 0 & -b_3 & -b_4 \\ a_3 & a_4 & (k_3 b_1 - \mu_0) & k_3 b_2 \\ -k_1 & 1 & (k_4 b_1 + k_2 b_3) & (k_4 b_2 + k_2 b_4 - \mu_0) \end{vmatrix}, \qquad [18]$$

where

$$k_j = \frac{\mu_j}{\mu_1}(\alpha^2 + m_j), \quad (j = 1, 2),$$

$$k_3 = 2\alpha^2(1 - \mu_0),$$

$$k_4 = \frac{2\alpha^2}{r_1}(1 - \mu_0) - i\alpha\ \mathrm{Re}_1 \frac{S_1}{1-c}.$$

To provide a non-trivial solution of the original problem [7]–[9], the determinant of $\mathbf{K}$ must be zero—which gives the required eigenvalue relation. In order to obtain a_k and b_k at $r = r_1$, the Runge–Kutta method is applied to integrate [14] and [15] and [16] and [17]. In actual computations, of course, an iterative procedure about c is performed until the determinant of $\mathbf{K}$ vanishes with some prescribed degree of accuracy.

It is worth noting that the boundary conditions at $r = r_2$ admit to form the functional relations between $v_2^{(k)}$ $(k = 1, 2, 3, 4)$ in a different way. However, [13] are chosen in such a way that the initial-value problem [16, 17] derived, can be solved with fewer computational difficulties.

4. NUMERICAL RESULTS AND DISCUSSION

(a) *Growth rate of the disturbances*

The growth rate of the disturbance $q = \mathscr{I}m(\alpha c)$ depends on a large parameters set: Re_1, We_1, $r_2 = R_2/R_1$, $\sigma_0 = \sigma_2/\sigma_1$, $\rho_0 = \rho_2/\rho_1$, $\mu_0 = \mu_2/\mu_1$ and α.

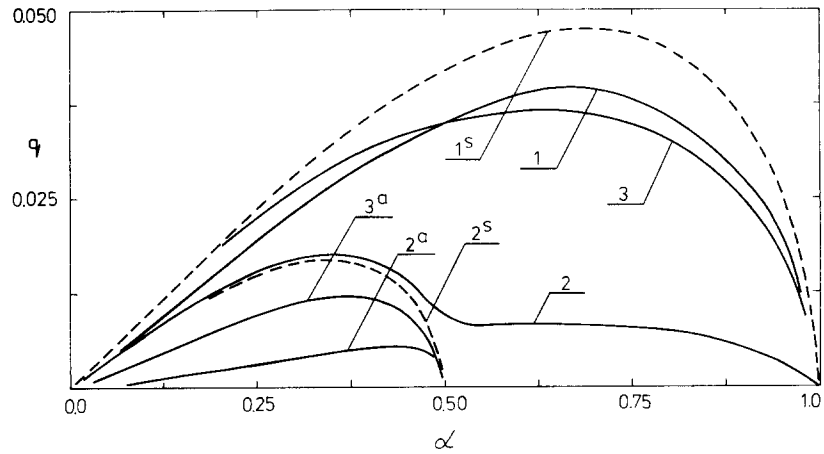

Figure 2. Growth rate q as a function of the wavenumber α in a comparison between compound jets and the corresponding single jets. ——, Compound jets with $\mathrm{Re}_1 = 500$, $\rho_0 = \mu_0 = 1$ and $r_2 = 2$: 1—$\mathrm{We}_1 = 50$, $\sigma_0 = 0$; 2, 2ᵃ—$\mathrm{We}_1 = 500$, $\sigma_0 = 10$; 3, 3ᵃ—$\mathrm{We}_1 = 50$, $\sigma_0 = 1$. ----, Single jets with $\mathrm{Re}_1 = 500$ and $\mathrm{We}_1 = 50$: 1ˢ—$r = r_1$; 2ˢ—$r = r_2$.

Figure 2 shows the growth rate q as a function of the wavenumber α. Typical examples of $q - \alpha$ curves, for the case of a compound jet with $\sigma_0 = \rho_0 = \mu_0 = 1$ and $r_2 = 2$, are curves 3 and 3ᵃ. Here $\mathrm{Re}_1 = 500$ and $\mathrm{We}_1 = 50$ are calculated for a primary jet of water: $\rho_1 = 997\ \mathrm{kg/m^3}$, $\mu_1 = 0.91$ cP, $\sigma_1 = 25$ dyn/cm, $R_1 = 166\ \mu\mathrm{m}$ and $U = 2.75$ m/s. In contrast to the single jet case, two families of unstable disturbances (curves 3 and 3ᵃ) are found in the long-wave area $\alpha < 1/r_2$. In the short-wave region, $1/r_2 < \alpha < 1$, only curve 3 represents unstable disturbances. Both families pass through a maximum. There is no positive q if $\alpha > 1$, and disturbances with such short wavelengths die away.

The existence of two families of unstable disturbances in the long-wave area is due to the existence of two surface tensions: the inner one at the interface between the phases; and the outer one at the surface of the compound jet. In support of this conclusion are the cases $1/\sigma_0 = 0$ and $\sigma_0 = 0$, i.e. $\sigma_1 = 0$ and $\sigma_2 = 0$, respectively. If $1/\sigma_0 = 0$, the compound jet is reduced to a single jet of radius $r = r_2$ (curve 2ˢ). Increasing the inner surface tension from zero, the second family of unstable disturbances appears in the long-wave region (see curve 2ᵃ), while the corresponding first family (curve 2) expands its unstable region from $\alpha < 1/r_2$ up to $\alpha < 1$. In the other extreme case, $\sigma_0 = 0$, one family of unstable disturbances exists also (curve 1). Here the secondary-fluid cover affects the growth rate q via inertial and viscous forces only, which explains the difference between curves 1 and 1ˢ. The latter corresponds to a single jet of the compound jet core.

To summarize, in the case of compound jets with $0 < \sigma_0 < \infty$ the first family of unstable disturbances is above the corresponding second family in the entire region, $0 < \alpha < 1$. Hence, the second family is irrelevant with regard to linear instability—therefore in the subsequent discussion and figures the second family of unstable disturbances will not be considered.

To study the influence of the secondary-fluid cover on the compound jet capillary instability we examine the primary jet with $R_1 = 166\ \mu\mathrm{m}$, $U = 2.75$ m/s, $\rho_1 = 997\ \mathrm{kg/m^3}$, $\mu_1 = 0.91$ cP, $\sigma_1 = 25$ dyn/cm and analyse the effect of the parameters σ_2, ρ_2, μ_2 and R_2, one by one, on the growth rate as a function of the wavenumber. In terms of the non-dimensional parameters this means that only one of σ_0, ρ_0, μ_0 and r_2 is varied whilst keeping the rest of the non-dimensional parameters, including Re_1 and We_1, constant. According to the assumption that the jet is destroyed by the most rapidly growing disturbance, the compound jet can become more or less stable depending on the maximum growth rate factor $q_* = \max_\alpha q$. Some of the examples included in the analysis are hard to study experimentally because of the large differences between the parameters of both phases, but they are shown in the figures to underline the tendencies observed in the phenomena.

(*b*) *Effect of the outer surface tension*

It is well-known that the most important factor for capillary instability is the surface tension, hence the existence of the co-axial cover is expected to affect the compound jet instability mainly via the outer surface tension.

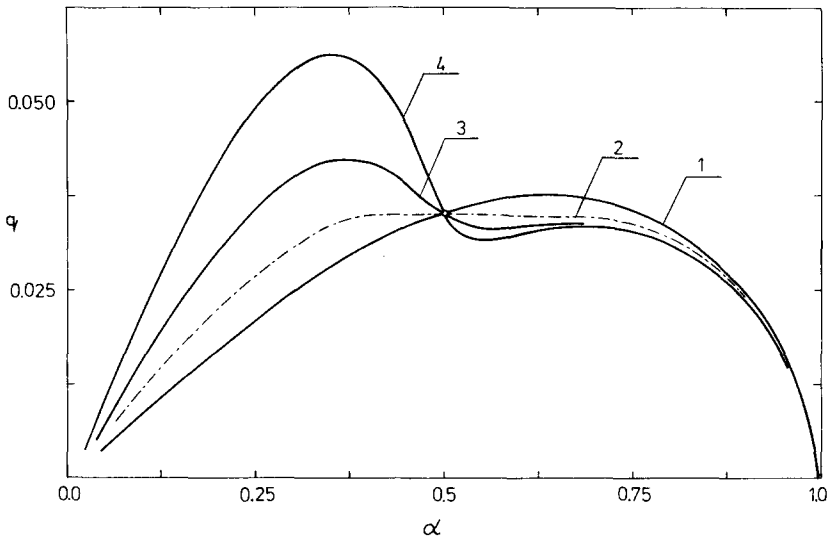

Figure 3. Effect of the outer surface tension on the growth rate q as a function of the wavenumber α ($\mathrm{Re}_1 = 500$, $\mathrm{We}_1 = 50$, $r_2 = 2$, $\rho_0 = \mu_0 = 1$): 1—$\sigma_0 = 0.5$; 2—$\sigma_0 = \sigma_{op} = 2.267$; 3—$\sigma_0 = 5$; 4—$\sigma_0 = 10$. The compound jet is the most stable among the jets with equal Re_1, We_1, ρ_0, μ_0 and r_2, if $\sigma_0 = \sigma_{op}$.

In figure 3 q–α curves are presented for the case of $\rho_0 = \mu_0 = 1$ and different values of σ_0. The outer surface tension influences the unstable disturbances in different ways depending on the wavenumber. In the long-wave area, $\alpha < 1/r_2$, the growth rate q increases with increasing σ_0, while σ_0 has a weak opposite effect on q in the short-wave region, $1/r_2 < \alpha < 1$. As is to be expected, the outer surface tension does not influence disturbances with wavelengths equal to the circumference of the compound jet and all q–α curves intercept at one and the same point, at $\alpha = 1/r_2$.

Increasing σ_0 from zero, the maximum growth rate factor q_* decreases and is shifted in the long-wave direction. It is worth computing the minimum value q_{op} of q_* as a function of σ_0. This case will correspond to that of the most stable jet among the compound jets with equal Re_1, We_1, ρ_0, μ_0 and r_2. In the example in figure 3 the minimum $q_{op} = 0.0335$ is reached at $\sigma_0 = \sigma_{op} = 2.267$ and $\alpha_{op} = 1/r_2$ (curve 2). Note that the growth rate of the disturbances around α_{op} in curve 2 is slightly below the maximum value q_{op} and this maximum is not clearly expressed in the figure. If $\sigma_0 > \sigma_{op}$, the q–α curves exhibit two local maxima and q_*, which now belongs to the long-wave area, $\alpha < 1/r_2$, increases with increasing σ_0 (see curves 3 and 4). The same effect was predicted by Sanz & Meseguer (1985), Radev & Shkadov (1985) and Shutov (1985) for the one-dimensional equation of motion for inviscid jets.

To summarize the results from figures 2 and 3 and the variety of numerical experiments not shown in the figures, the capillary instability of compound jets under short-wave disturbances, $1/r_2 < \alpha < 1$, is governed mainly by the inner surface tension; while in the long-wave region, $\alpha < 1/r_2$, the influence of the outer surface tension dominates.

(*c*) *Effect of the secondary-fluid density and viscosity*

Figures 4 and 5 show the effect of the secondary-fluid density and viscosity on the growth rate factor, respectively. The primary jet is assumed to be the same as in figure 3 and σ_0 is taken as equal to 1. The influence of ρ_0 and μ_0 is spread over the entire range of $0 < \alpha < 1$ and has a unidirectional effect: the compound jet is more stable with increased value of the secondary-fluid density or viscosity. The qualitative difference between the influence of ρ_0 and μ_0 lies in the following. For large ρ_0 the q–α curves exhibit only one local maximum which belongs to the short-wave area, $1/r_2 < \alpha < 1$ (figure 4, curves 1 and 2). Upon decreasing ρ_0, the second local maximum appears in the region $\alpha < 1/r_2$ (in figure 4 it occurs when $\rho_0 < 0.1767$) but it is still less than the maximum in the short-wave area (figure 4, curve 3). If the density ratio reaches a critical value, both maxima become equal (figure 4, curve 4). Beyond this critical value the maximum growth rate factor q_* belongs to $\alpha < 1/r_2$ (figure 4, curve 5), as it does in the case of $\sigma_0 > \sigma_{op}$ (see

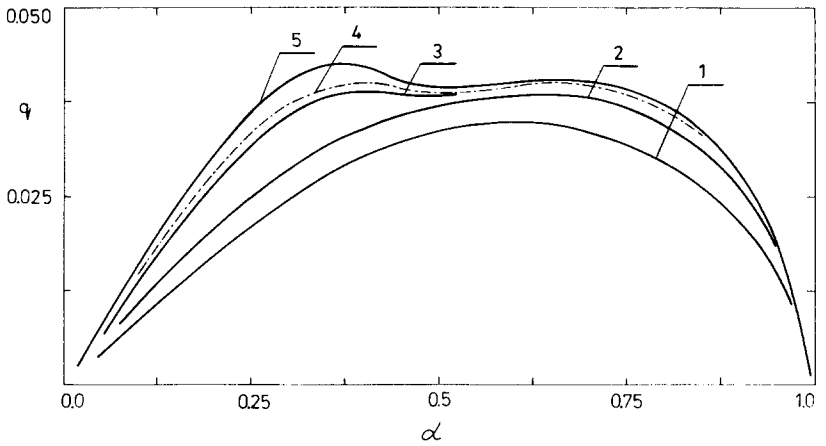

Figure 4. Effect of the secondary-fluid density on the growth rate q as a function of the wavenumber α ($Re_1 = 500$, $We_1 = 50$, $r_2 = 2$, $\sigma_0 = \mu_0 = 1$): 1—$\rho_0 = 2$; 2—$\rho_0 = 0.5$; 3—$\rho_0 = 0.16$; 4—$\rho_0 = 0.1385$; 5—$\rho_0 = 0.1$. The compound jet is more stable with increased secondary-fluid density. If $\rho_0 = 0.1385$ both maxima in the $q - \alpha$ curve are equal.

figure 3). Similar effects are not observed upon decreasing μ_0 (see figure 5), which shows that the influence of μ_0 on the capillary instability is weaker than that of ρ_0.

(d) Effect of the thickness of the secondary-fluid layer

In figure 6 the effect of the thickness of the secondary-fluid layer is illustrated for the case of $\sigma_0 = \rho_0 = \mu_0 = 1$.

When $r_2 \geqslant 5$ the outer surface tension has no effect and the q–α curves are indistinguishable from one another (curve 4). The results are the same as in the case of a single jet of the core interacting with the unbounded medium of a secondary fluid if both phases stream with uniform undisturbed velocity. Upon decreasing the thickness of the secondary-fluid layer (curves 3, 2 and 1), the outer surface tension comes into effect and the compound jet becomes less stable. In the case of a thin layer, $r_2 \sim 1$ (e.g. curve 1), the effects of both surface tensions sum up, i.e. the growth rate q approaches the results for a corresponding single jet with surface tension equal to the sum of the inner and outer ones (curve 1^s).

(e) Regimes of break-up and break-up length

The compound jet configuration is destroyed due to propagation of the most rapidly growing

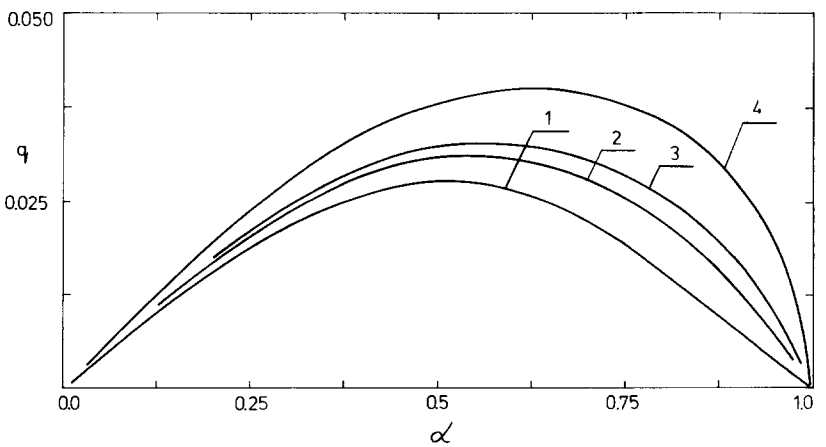

Figure 5. Effect of the secondary-fluid viscosity on the growth rate q as a function of the wavenumber α ($Re_1 = 500$, $We_1 = 50$, $r_2 = 2$, $\sigma_0 = \rho_0 = 1$): 1—$\mu_0 = 50$; 2—$\mu_0 = 20$; 3—$\mu_0 = 10$; 4—$\mu_0 = 0.1$. The compound jet is more stable with increased secondary-fluid viscosity.

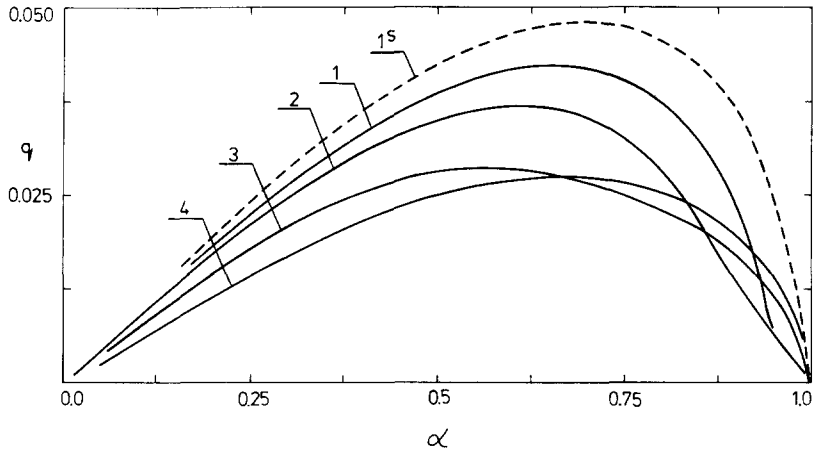

Figure 6. Effect of the thickness of the secondary-fluid layer on the growth rate q as a function of the wavenumber α. ——, Compound jets with $Re_1 = 500$, $We_1 = 50$ and $\sigma_0 = \rho_0 = \mu_0 = 1$: 1—$r_2 = 1.1$; 2—$r_2 = 1.25$; 3—$r_2 = 1.67$; 4—$r_2 \geqslant 5$. ----, Single jet with $Re_1 = 500$, $We_1 = 100$ and radius $r = r_1$. The compound jet is more stable with increased thickness of the secondary-fluid layer. In the case of a very thin layer, the effects of both surface tensions sum up.

disturbance with a growth rate q_* at the point where the primary jet or its cover is no longer a coherent portion. The distance to this first break-up point is determined by the following:

$$L = \min\{L_1, L_2\}, \quad L_1 = \frac{1}{q_*}\ln\left(\frac{R_1}{\delta_1}\right), \quad L_2 = \frac{1}{q_*}\ln\left(\frac{R_2 - R_1}{\delta_2 - \delta_1}\right), \qquad [19]$$

where $\delta_j = |H_j| R_1$ is the initial disturbance amplitude at the surface $r = R_j$ and L_1 and L_2 (normalized against R_1) are the break-up lengths of the core and its cover, respectively. Note that neither δ_1 or δ_2 can be chosen arbitrarily. To determine δ_1 as a function of δ_2, the eigenfunction $v_2^{(1)}$ has to be computed at $r = r_1$, using [10] and the backward procedure in [13], when $v_2^{(1)}$ is given an initial value at $r = r_2$.

It should be noted that the present theory is valid up to the distance L as long as the compound jet configuration still exists.

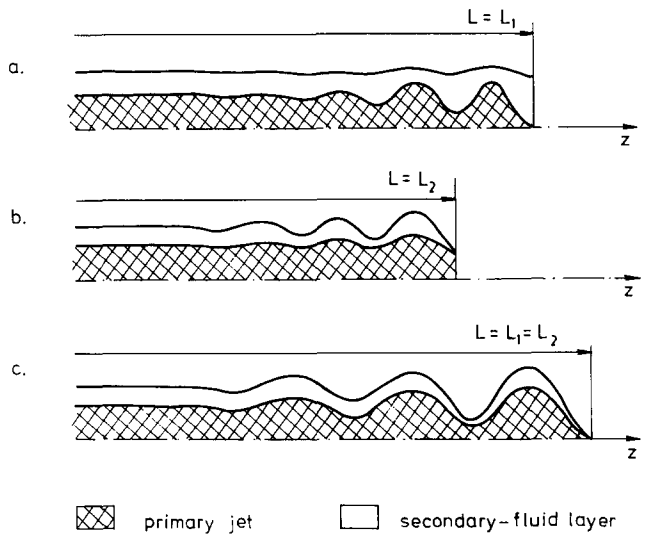

Figures 7a–c. Capillary break-up regimes of compound jets. (a) Drop formation within the outer fluid. The core breaks up first while its layer still exists as a coherent portion. (b) Break-up by meeting of interfaces. The cover cuts off before the core. (c) Break-up as a single jet. Both phases break up simultaneously at one and the same point.

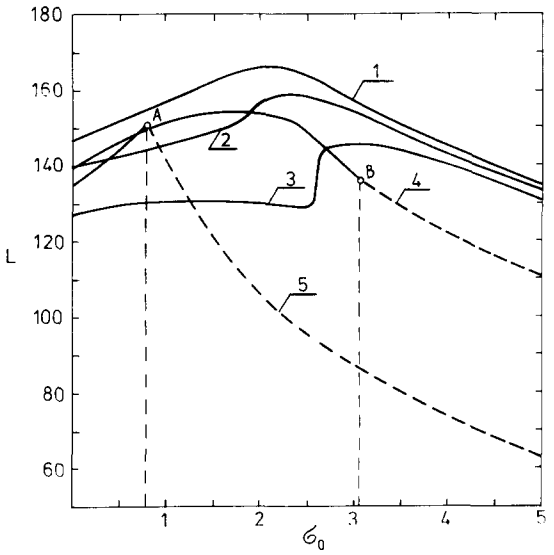

Figure 8. Break-up length L as a function of the surface tension ratio σ_0[$\mathrm{Re}_1 = 87.12$, $\mathrm{We}_1 = 9.05$, $r_2 = 2.03$, $\ln(R_2/\delta_2) = 13.4$]: 1—$\rho_0 = 1$, $\mu_0 = 1$; 2—$\rho_0 = 1$, $\mu_0 = 0.5$; 3—$\rho_0 = 1$, $\mu_0 = 0.1$; 4—$\rho_0 = 0.5$, $\mu_0 = 1$; 5—$\rho_0 = 0.1$, $\mu_0 = 1$. All break-up regimes prove to be feasible: ——, Drop formation within the outer fluid ($L = L_1$); ----, break-up by meeting of interfaces ($L = L_2$); ○, breakup as a single jet ($L = L_1 = L_2$).

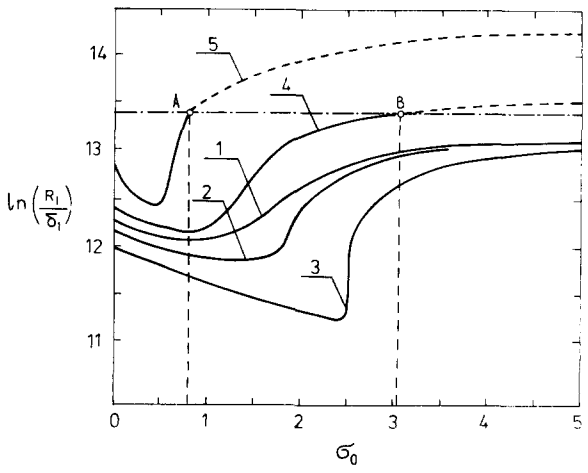

Figure 9. The corresponding initial disturbance level $\ln(R_1/\delta_1)$ at the interfacial surface as a function of the surface tension ratio σ_0. The horizontal axial line $\ln(R_1/\delta_1) = \ln(R_2/\delta_2)$ separates the break-up regimes.

In figures 7a–c three possible regimes of a compound jet break-up are shown. In figure 7a the primary jet breaks earlier than its cover (drop formation within the outer fluid, $L = L_1$). In figure 7b the cover cuts off while the primary jet still exists as a coherent portion (break-up by meeting of interfaces, $L = L_2$). In the extreme case, figure 7c, the primary jet and its cover break up simultaneously at one and the same point (break-up as in the single jet case, $L = L_1 = L_2$).

The numerical experiments are performed on the basis of the compound jet shown in figure 6 from Hertz & Hermanrud (1983). For the primary jet of 80% H_2O + 20% glycerol ($R_1 = 66.5\,\mu$m, $R_2 = 135\,\mu$m, $U = 2.6$ m/s, $\rho_1 = 1047$ kg/m^3, $\mu_1 = 2.078$ cP, $\sigma_1 = 52$ dyn/cm) we have $\mathrm{Re}_1 = 87.12$, $\mathrm{We}_1 = 9.05$ and $r_2 = 2.03$. The break-up length L is plotted in figure 8 as a function of the surface tension ratio σ_0 for the case of differing viscosity and density of the outer fluid. A constant value of 13.4 is assumed for $\ln(R_2/\delta_2)$, a value quoted by Grant & Middleman (1966) for single jets. It is seen from the figure that all regimes of break-up prove to be feasible in the numerical experiments. The continuous curves correspond to the case in figure 7a, whereas the dashed curves represent the regime in figure 7b. At points A and B, where σ_0 takes the critical values $\sigma_{cr} = 0.8050$ and 3.075 respectively, the compound jets break up as single jets (see figure 7c) regardless of the differing densities of the two phases.

The corresponding initial disturbance level $\ln(R_1/\delta_1)$ at the interface $r = r_1$ is shown in figure 9. The occurrence of any break-up regime can be predicted by comparing the ratios R_1/δ_1 and R_2/δ_2. All examples below the horizontal axial line $\ln(R_1/\delta_1) = 13.4$ in figure 9 correspond to figure 7a

$$\left(\frac{R_1}{\delta_1} < \frac{R_2}{\delta_2}\right).$$

Above this line the break-up regime shown in figure 7b is manifested

$$\left(\frac{R_1}{\delta_1} > \frac{R_2}{\delta_2}\right).$$

At points A and B, where the horizontal axial line intercepts curves 4 and 5, break-up as a single jet occurs

$$\left(\frac{R_1}{\delta_1} = \frac{R_2}{\delta_2}\right).$$

Figures 8 and 9 and all numerical experiments (not shown here), performed for a large variety of the parameters, are in support of the following conclusions:

(i) If the compound jet is formed from a primary jet of density less than or equal to the density of the secondary-fluid cover ($\rho_0 \geqslant 1$), then only drop formation within the outer fluid occurs, regardless of the differing viscosities and surface tensions of the two phases.

(ii) If the density of the primary jet is greater than the density of the secondary-fluid cover ($\rho_0 < 1$), all break-up regimes are possible. Assuming constant values of Re_1, We_1, r_2 and μ_0, the analysis gives:
—break-up as a single jet if σ_0 is equal to a certain critical value σ_{cr};
—drop formation within the outer fluid if $\sigma_0 < \sigma_{or}$;
—break-up by meeting of interfaces if $\sigma_0 > \sigma_{cr}$.
The critical value σ_{cr} is dependent on a combination of all jet parameters so it has not yet been possible to determine the correlation between jet parameters and σ_{cr}.

(iii) The break-up length L reaches a maximum value at $\sigma_0 = \sigma_{op}$, assuming constant values for Re_1, We_1, r_2, ρ_0, μ_0 and $\ln(R_1/\delta_1)$.

More often than not, the first break-up regime—drop formation within the outer fluid—occurs. This can be explained in the following way. The primary jet is bounded by a capillary surface with a curvature greater than the curvature of the compound jet itself, so more often it is the core that breaks up first. To manifest the second regime—break-up by meeting of interfaces—it is necessary that the outer surface tension be sufficiently great, but this alone is not enough. The compound jet can not undergo the second break-up regime even if the outer surface tension increases to infinity. In this case the behaviour of the compound jet approaches that of break-up as a single jet, but the compound jet break-up is still in the first regime, because the destabilizing effect of the outer surface tension influences the jet core as well. The outer surface tension can come into effect across the secondary-fluid cover faster, and cause its cut-off before the core breaks up into drops, only if the density of the cover is less than the density of the core.

5. EXPERIMENTS VERSUS THEORY

Due to the scarcity of experimental data in the literature the comparison is made only for the low-viscous jets studied by Hertz & Hermanrud (1983). Two different compound jets were considered. In the first example (figure 5 of Hertz & Hermanrud) the compound jet consists of one and the same mixture 80% H_2O + 20% glycerol but the primary jet is dyed. From the data quoted by Hertz & Hermanrud ($R_1 = 66.5\,\mu$m, $R_2 = 135\,\mu$m, $U = 2.6$ m/s, $\mu_1 = \mu_2 = 2.078$ cP, $\rho_1 = \rho_2 = 1047$ kg/m^3, $\sigma_1 = 0$, $\sigma_2 = 72$ dyn/cm), we have $\mathrm{Re}_1 = 87.12$, $\mathrm{We}_1/\sigma_0 = 6.537$, $1/\sigma_0 = 0$, $r_2 = 2.03$ and $\rho_0 = \mu_0 = 1$. As expected, the compound jet behaves as a single homogeneous jet and the theory gives $\mathrm{L} = \mathrm{L}_1 = \mathrm{L}_2$. On the basis of the compound jet length $\mathrm{L} = 331$ (22 mm measured by Hertz & Hermanrud) the back-calculated value of the initial disturbance level is $\ln(R_2/\delta_2) = 14.74$. The value of the wavenumber $\alpha_* = 0.3361$, corresponding to the most rapidly growing disturbance, is in good agreement with the value $\alpha_* = 0.3379$, corresponding to the last half-wavelength of 0.62 mm measured in figure 5c of Hertz & Hermanrud (1983). Sanz & Meseguer (1985) report a value of 0.3458 in the case of an inviscid analysis of the same example.

Whereas the example above shows the validity of the analysis for single homogeneous jets only, the example in figure 6 of Hertz & Hermanrud is more interesting for the purpose of comparison. The primary jet is of the same mixture, while the secondary fluid is a dimethyl silicone oil which creates a difference only in $\sigma_1 = 52$ dyn/cm and $\sigma_2 = 20$ dyn/cm. Hence $\mathrm{Re}_1 = 87.12$, $\mathrm{We}_1 = 9.051$, $r_2 = 2.03$, $\sigma_0 = 0.3846$ and $\rho_0 = \mu_0 = 1$. Here, both experimentally and numerically, we have drop formation within the outer liquid. Hertz & Hermanrud make no comment about the break-up length L and our comparison concerns the wavenumber α_* only. The numerical result is

$\alpha_* = 0.6816$, whereas the value corresponding to the last 0.6 mm wave in figure 6a of Hertz & Hermanrud (1983) is $\alpha_* = 0.6964$. The analysis of Sanz & Meseguer (1985) predicts $\alpha_* = 0.6793$.

Hertz & Hermanrud (1983) used liquids of approximately equal densities and the second regime, break-up by meeting of interfaces, was not feasible in their experiments.

6. CONCLUSION

The temporal capillary instability of axisymmetrical compound jets was studied via axisymmetrical travelling waves with amplitudes small enough to use linear analysis.

If the undisturbed velocity profile is assumed homogeneous and uniform, the phase velocity of the disturbances can be obtained analytically, but the solution is in a rather complicated form in terms of Bessel functions and is difficult to use in the analysis.

In the present paper a numerical solution of the boundary-value problems for the Orr–Sommerfeld equations was proposed. The initial-value technique applied allowed high accuracy of the order 10^{-5}–10^{-6} in the computations and was applicable to the entire range of Reynolds numbers—which includes all laminar compound jets of liquids with differing density, viscosity and surface tension values. It could also be applied in the case of a non-uniform undisturbed velocity profile, studied by Radev & Gospodinov (1986), which makes it possible to include the effect of velocity-profile relaxation in future numerical analyses.

Since the compound jet has a large number of parameters, it is difficult to investigate all their possible combinations. It was shown that the capillary instability of the compound jets is governed mainly by the surface tensions on the two surfaces. Two families of disturbances with growing amplitudes were found but the jet instability is controlled only by the family possessing the larger growth rate of disturbances. The next important parameter was the density ratio, the viscosity ratio has a comparatively weak influence on compound jet instability.

According to the way in which the initial compound jet configuration is destroyed, three different regimes of break-up were predicted numerically. The linear analysis gives only the distance L to the first break-up point, as was shown in figures 7a–c. In the general case, the determination of the final point of drop formation, where the compound jet itself breaks up, requires further study of the phenomena.

The numerical results concerning the wavenumber of the most rapidly growing disturbance are in good agreement with the experimental data of Hertz & Hermanrud (1983). As regards the comparison of the break-up length L, there is no experimental data available except for homogeneous compound jets.

In the literature there is no mention of experimental evidence of the second break-up regime: capillary break-up by meeting of interfaces. It was predicted numerically when both phases exhibited comparatively large differences in density or surface tension. Actually, if such compound jets are examined experimentally, it might be possible for the sinuous or varicose instability to grow faster than the capillary one. This could be an interesting point for future study, both experimentally and theoretically.

REFERENCES

ABRAMOV, A. A., BIRGER, E. S., KONYUKHOVA, N. B. & ULJANOVA, V. I. 1977 On methods of numerical solution of boundary value problems for systems of linear ordinary differential equations. *Colloquia Mathematica Societatis Janos Bolyai.* Keszthely, Hungary. *Numerical Methods*, Vol. 22, pp. 33–67. North-Holland, Amsterdam.

GRANT, R. P. & MIDDLEMAN, S. 1966 Newtonian jet stability. *AIChE Jl* **12,** 671–678.

HERMANRUD, B. 1981 The compound jet. A new method to generate fluid jets for ink printing. Report 1/1981, LUTEDX/(TEEM-1006)], pp. 1–143. Lund Institute of Technology, Lund, Sweden.

HERMANRUD, B. & HERTZ, C. H. 1979 Ink jet development at the Lund Institute of Technology. *J. appl. photogr. Engng* **5,** 220–225.

HERTZ, C. H. & HERMANRUD, B. 1983 A liquid compound jet. *J. Fluid Mech.* **131,** 271–287.

RADEV, S. P. 1986 Lateral instability of two-layer liquid capillary jets. *Theor. appl. Mech.* **1,** 45–54 (in Russian).

RADEV, S. P. & GOSPODINOV, P. 1986 Numerical treatment of the steady flow of a liquid compound jet. *Int. J. Multiphase Flow* **12,** 997–1007.

RADEV, S. P. & SHKADOV, V. 1985 On the stability of two-layer capillary jets. *Theor. appl. Mech.* **3,** 68–75 (in Russian).

SANZ, A. & MESEGUER, J. 1985 One-dimensional linear analysis of the compound jet. *J. Fluid Mech.* **159,** 55–68.

SHUTOV, A. A. 1985 Instability of capillary liquid compound jets. *Mech. Jidkosti Gasa.* **4,** 3–8 (in Russian).

TAYFER, J. 1973 *Lösung der Randwertprobleme für systeme von linearen Differentialgleichungen.* Academia, Praha.

TOMOTIKA, S. 1935 On the instability of a cylindrical thread of a viscous liquid surrounded by another viscous fluid. *Proc. R. Soc. Lond.* **A150,** 322–337.

WEBER, C. 1931 Zum Zerfall eines Flüssigkeitsstrahles. *Z. angew. Math. Mech.* **11,** 136–141.